Lawrence Berkeley National Laboratory

Title
SN 2018ijp: the explosion of a stripped-envelope star within a dense H-rich shell?★★★

Permalink
https://escholarship.org/uc/item/9959z3qr

Authors
Tartaglia, L
Sollerman, J
Barbarino, C
et al.

Publication Date
2021-06-01

Peer reviewed

SN 2018ijp: the explosion of a stripped-envelope star within a dense H-rich shell?[*],[**]

L. Tartaglia[1,2], J. Sollerman[1], C. Barbarino[1], F. Taddia[1], E. Mason[3], M. Berton[4,5], K. Taggart[6], E. C. Bellm[7], K. De[8], S. Frederick[9], C. Fremling[10], A. Gal-Yam[11], V. Z. Golkhou[7,12], M. Graham[10], A. Y. Q. Ho[8], T. Hung[13], S. Kaye[14], Y.-L. Kim[15], R. R. Laher[16], F. J. Masci[16], D. A. Perley[6], M. D. Porter[14], D. J. Reiley[14], R. Riddle[14], B. Rusholme[16], M. T. Soumagnac[17,11], R. Walters[10,14]

1. Department of Astronomy and the Oskar Klein Centre, Stockholm University, AlbaNova, SE 106 91 Stockholm, Sweden
   (e-mail: leonardo.tartaglia@astro.su.se)
2. INAF - Osservatorio Astronomico di Padova, Vicolo dell'Osservatorio 5, I-35122 Padova, Italy
3. INAF - Osservatorio Astronomico di Trieste, Via G.B. Tiepolo, 11, I-34143 Trieste, Italy
4. Finnish Centre for Astronomy with ESO (FINCA), University of Turku, Vesilinnantie 5, FI-20014 University of Turku, Finland
5. Aalto University Metsähovi Radio Observatory, Metsähovintie 114, FI-02540 Kylmälä, Finland
6. Astrophysics Research Institute, Liverpool John Moores University, IC2, Liverpool Science Park, 146 Brownlow Hill, Liverpool L3 5RF, UK
7. DIRAC Institute, Department of Astronomy, University of Washington, 3910 15th Avenue NE, Seattle, WA 98195, USA
8. Cahill Center for Astrophysics, California Institute of Technology, MC 249-17, 1200 E California Boulevard, Pasadena, CA 91125, USA
9. Department of Astronomy, University of Maryland, College Park, MD 20742, USA
10. Division of Physics, Mathematics and Astronomy, California Institute of Technology, Pasadena, CA 91125, USA
11. Department of Particle Physics and Astrophysics, Weizmann Institute of Science, 234 Herzl St., Rehovot, 76100, Israel
12. The eScience Institute, University of Washington, Seattle, WA 98195, USA
13. Department of Astronomy and Astrophysics,University of California, Santa Cruz, California, 95064, USA
14. Caltech Optical Observatories, California Institute of Technology, Pasadena, CA 91125 USA
15. Université de Lyon, Université Claude Bernard Lyon 1, CNRS/IN2P3, IP2I Lyon, F-69622, Villeurbanne, France
16. IPAC, California Institute of Technology, 1200 E. California Blvd, Pasadena, CA 91125, USA
17. Lawrence Berkeley National Laboratory, 1 Cyclotron Road, Berkeley, CA 94720, USA

ABSTRACT

In this paper, we discuss the outcomes of the follow-up campaign of SN 2018ijp, discovered as part of the Zwicky Transient Facility survey for optical transients. Its first spectrum shows similarities to broad-lined Type Ic supernovae around maximum light, whereas later spectra display strong signatures of interaction between rapidly expanding ejecta and a dense H-rich circumstellar medium, coinciding with a second peak in the photometric evolution of the transient. This evolution, along with the results of modeling of the first light curve peak, suggests a scenario where a stripped star exploded within a dense circumstellar medium. The two main phases in the evolution of the transient could be interpreted as a first phase dominated by radioactive decays, and an later interaction-dominated phase where the ejecta collide with a pre-existing shell. We therefore discuss SN 2018jp within the context of a massive star depleted of its outer layers exploding within a dense H-rich circumstellar medium.

Key words. Supernovae: general – Supernovae: individual: SN 2018ijp, ZTF18aceqrrs

1. Introduction

A supernova (SN) is the most spectacular way a star can end its life, where progenitors more massive than $8 - 9\,M_\odot$ (see, e.g., Heger et al. 2003; Smartt 2009) are expected to explode as core-collapse (CC) SNe.
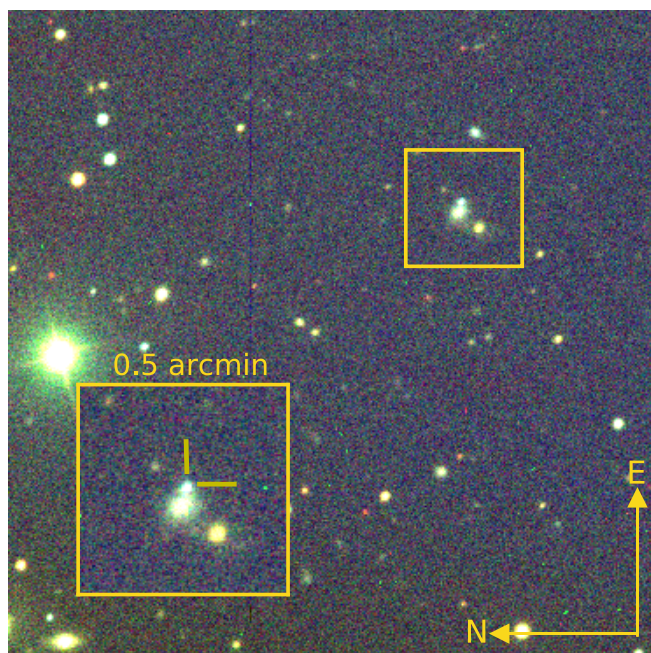
SNe interacting with a dense circumstellar medium (CSM) can produce a wide range of observables, resulting in a large heterogeneity of photometric and/or spectroscopic properties. The classification of interacting transients is typically based on the presence of narrow emission features in their spectra, with Type IIn (Schlegel 1990) or Ibn (Pastorello et al. 2016; Hosseinzadeh et al. 2019) SNe being those showing prominent narrow H or He lines, respectively.

The current picture for the most common narrow-lined interacting SNe is that of fast moving ejecta colliding with a slow-moving dense CSM. In the shocked regions, a characteristic "forward-reverse" shock structure forms (e.g., Chevalier 1982; Chevalier & Fransson 1994), and energetic photons can ionize the surrounding medium giving rise to the structured, multi-component emission line profiles usually observed in SNe IIn (see, e.g., Turatto et al. 1993; Chugai & Danziger 1994; Taddia et al. 2020). In this context, narrow emission lines (full–width–at–half–maximum – FWHM – of a few $10^2\,\mathrm{km\,s^{-1}}$) are recombination lines produced in the slow-moving, un-shocked CSM.

---

[*] Photometric tables are only available at the CDS via anonymous ftp.
[**] Spectroscopic data are available through the Weizmann Interactive Supernova Data Repository (WISeREP).

Fig. 1. Color image of the field of SN 2018ijp, obtained combining $g-$, $r-$ and $i-$band frames obtained on 2019 January 26 with LT. SN 2018ijp is the the blue source in the middle of the inset.

This requires the presence of a dense CSM produced by the progenitor star prior to its explosion, and seems to suggest massive luminous blue variables (LBVs, see, e.g., Trundle et al. 2008; Gal-Yam & Leonard 2009), red supergiants (RSG) with super-winds (see, e.g., Smith et al. 2009; Yoon & Cantiello 2010) or Wolf-Rayet (WR) stars in binary systems (e.g., Maund et al. 2016) as candidate progenitors for SNe IIn and Ibn. Such stars are all able to provide the environment required to produce the signatures of interaction (see Humphreys & Davidson 1994; Crowther 2007). This scenario is also supported by observations of eruptive episodes occurring weeks to years prior to the explosion of the star as an interacting SN (Foley et al. 2007; Pastorello et al. 2007, 2013; Ofek et al. 2014a; Tartaglia et al. 2016).

On the other hand, ejecta-CSM interaction can occur in many kinds of explosions or stellar outbursts and may prevent the observer to gain insight on the intrinsic nature of the transient, including the explosion mechanism triggering the SN explosion. This is the case for the sub-class of interacting transients known as SNe Ia-CSM (see, e.g., Silverman et al. 2013), which are believed to be thermonuclear explosions embedded in a dense H-rich medium.

Signatures of interaction, occasionally delayed with respect to the SN explosion, have been observed also in stripped-envelope (SE) SNe, optical transients typically showing a lack of H (SNe IIb and Ib) or both H and He features (SNe Ic) in their optical spectra. A few recent examples of SE SNe showing this evolution are SNe 2014C (Milisavljevic et al. 2015; Margutti et al. 2017), 2017dio (Kuncarayakti et al. 2018), 2017ens (Chen et al. 2018) and SNe 2019tsf and 2019oys (Sollerman et al. 2020). These can be interpreted as CC explosions of SE SNe within a dense, H-rich medium, with a possible progenitor scenario being that of a massive CSM produced during the RSG stage or by a stellar companion (e.g., Milisavljevic et al. 2015).

In this context, we present the discovery and discuss the results of our follow-up campaign of SN 2018ijp, discovered as part of the Zwicky Transient Facility (ZTF; Graham et al. 2019; Bellm et al. 2019; Masci et al. 2019) during the first year of operations. The transient was discovered in the host SDSS J102137.72+085554.1 (Fig. 1) on 2018 November 7.41 UT and labelled ZTF18aceqrrs[1]. The photometric and spectroscopic follow-up campaigns were triggered soon after discovery through the GROWTH 'Marshal' (Kasliwal et al. 2019). A description of the facilities used and the reduction steps performed to obtain final light curves and spectra are described in Sect. 2. SN 2018ijp shows a relatively fast photometric evolution with double-peaked $g-$ and $r-$band light curves. The spectra show strong signatures of delayed interaction with a dense pre-existing H-rich CSM in the form of narrow H lines in emission increasing their strength with time and a spectral continuum becoming significantly bluer with time, as described in Sect. 3. While interaction features dominate the evolution of SN 2018ijp at later times, we note that the spectrum around the first peak resembles those typical of a subclass of broad-lined Type Ic SNe (Ic-BL SNe; see, e.g., Taddia et al. 2019, and references therein), with a good match with several Type Ic/Ic-BL SNe. In addition, modeling the first peak in the context of a radioactively powered light curve gives ^{56}Ni and total ejected masses comparable with those obtained for the Type Ic-BL SN iPTF15dqg (Taddia et al. 2019). In Sect. 3 and 4, we therefore discuss the observables of SN 2018ijp in the context of a massive, SE star within a dense H-rich medium. A brief summary of our main conclusions is reported in Sect. 5.

In the following, we adopt a foreground Galactic extinction $E(B - V) = 0.029$ mag along the line of sight of SN 2018ijp, as estimated by Schlafly & Finkbeiner (2011) using a standard extinction law (Cardelli et al. 1989) with $R_V = 3.1$. We did not include any additional contribution from the local environment to the total extinction, since we could not identify strong Na ID features at the redshift of the host in the spectra of SN 2018ijp (see Sect. 3.2). The distance to SN 2018ijp was computed from the redshift derived using host lines (see Sect. 3.2) assuming a standard cosmology with H$_0$ = 73 km s^{-1} Mpc^{-1}, Ω_M = 0.27 and Ω_Λ = 0.73, resulting in a luminosity distance $D_L = 373$ Mpc[2].

2. Observations and data reduction

Photometry of the transient was mostly obtained using the Samuel Oschin telescope (P48) with the ZTF camera (Dekany et al. 2020) in g and r bands. Additional photometry was obtained with the Nordic Optical Telescope (NOT) using the Alhambra Faint Object Spectrograph and Camera (ALFOSC[3]). P48 frames were obtained through the NASA/IPAC Infrared Science Archive[4], while magnitudes for these data were obtained using the dedicated pipeline SNOoPY[5] performing point-spread-function (PSF) photometry on template subtracted images. Templates and magnitudes of the reference stars were obtained from the Sloan Digital Sky Survey Data Release 14 (DR14; Abolfathi et al. 2018) available through the SDSS Catalog Archive Server (CAS[6]). Three additional *gri* epochs were obtained using the Liverpool Telescope (LT; Steele et al. 2004) with the optical imaging component of the Infrared-Optical (IO) suite of instruments (IO:O[7]). LT data reduction was performed through a

---

[1] https://lasair.roe.ac.uk/object/ZTF18aceqrrs/
[2] Derived using CosmoCalc (Wright 2006) available at: http://www.astro.ucla.edu/~wright/CosmoCalc.html
[3] http://www.not.iac.es/instruments/alfosc/
[4] https://irsa.ipac.caltech.edu/Missions/ztf.html
[5] http://graspa.oapd.inaf.it/snoopy.html
[6] https://www.sdss.org/dr14/data_access/tools/
[7] https://telescope.livjm.ac.uk/TelInst/Inst/IOO/

Table 1. Log of the spectroscopic observations of SN 2018ijp

Date	JD	Phase (d)	Instrumental setup	Grism/Grating	Spectral range (Å)	Resolution ($\lambda/\Delta\lambda$)	Exposure time (s)
20181201	2458454.08	+24	Keck1+LRIS	400/3400+400/8500	$3500 - 9500$	900	$300 + 300$
20190115	2458498.64	+65	NOT+ALFOSC	Gr4	$4000 - 9500$	300	2700
20190201	2458516.03	+81	Keck1+LRIS	400/3400+400/8500	$3500 - 9500$	860	$600 + 600$
20190204	2458519.58	+84	NOT+ALFOSC	Gr4	$4000 - 9500$	320	2700
20190227	2458542.44	+105	NOT+ALFOSC	Gr4	$4000 - 9500$	400	2×2700
20190403	2458576.89	+137	Keck1+LRIS	400/3400 + 400/8500	$3500 - 9500$	800	$300 + 300$
20190504	2458607.56	+165	VLT+Xshooter	UVB+VIS+NIR	$3500 - 20000$	$5400 + 8900 + 5600$	$3 \times (1200 + 1262 + 300)$
20200124	2458873.02	+410	Keck1+LRIS	400/3400 + 400/8500	$3500 - 9500$	850	1375

Notes. The resolution of each spectrum was estimated from [O I] sky lines. Rest frame phases refer to the estimated epoch of the explosion. NOT: 2.56 m Nordic Optical Telescope with ALFOSC; VLT: 8 m Very Large Telescope with X-shooter (ESO Observatorio del Paranal, Chile); KECK: 10 m Keck I telescope with LRIS (Mauna Kea Observatory, Hawaii, U.S.A.). Data will be released through WISEREP.

dedicated pipeline, using PSF photometry obtained on template subtracted images. Templates and magnitudes of the photometric standards used were provided by the Pan-STARRS1 (PS1) survey (Tonry et al. 2012). One point of $i-$band photometry (on 2018 December 24.36 UT) was obtained using the Palomar 60-inch telescope (P60) with the SED Machine (SEDM; Ben-Ami et al. 2012; Blagorodnova et al. 2018) and reduced using the FPIPE pipeline (Fremling et al. 2016).

A log of the spectroscopic observations is reported in Table 1, including the names of the instruments used and basic information about the spectra. The classification spectrum, along with three additional spectra, were obtained with the Keck-I telescope using the Low Resolution Imaging Spectrograph (LRIS; Oke et al. 1994) and reduced using the automated pipeline LPIPE (Perley 2019). Three additional spectroscopic observations were performed using the NOT with ALFOSC, reduced using FOScGUI[8]. An additional intermediate resolution spectrum was obtained using the ESO Very Large Telescope (VLT) with the X-shooter (Vernet et al. 2011), echelle spectrograph[9] and reduced using the ESO dedicated pipeline through the ESOREX v3.2.0 (ESO CPL Development Team 2015) and GASGANO environments.

3. Analysis and discussion

3.1. Photometry

Pre-SN observations of the field of SN 2018ijp were obtained by ZTF since 2018 March 31.3 UT, resulting in no detections down to average magnitudes of $\simeq 21$ mag in both g and r bands. Last non-detection limits were obtained on 2018 November 4.5 UT (corresponding to $g > 20.6$ and $r > 21.4$ mag), roughly three days before the first $g-$ and $r-$band detections. We will therefore adopt 2018 November 6.0 UT (JD $= 2458428.5 \pm 1.5$, the mid-point between the first detection and the last non-detection limit) as an estimate of the explosion epoch of SN 2018ijp and refer to phases with respect to this date. Magnitudes at rest frame epochs were obtained computing k-corrections using the spectra of SN 2018ijp and following the prescriptions of Hogg et al. (2002, see their Eq. 13), adopting a recessional velocity of $cz = 25540$ km s^{-1}, as derived from the redshift estimated from the host lines in the X-shooter spectrum ($z = 0.0852$; see Sect. 3.2.2). The resulting gri light curves are shown in Fig. 2 (left panel), along with an estimate of the bolometric luminosity of SN 2018ijp (right panel), which will be discussed below.

The early photometric evolution is fast, with both $g-$ and $r-$band light curves rapidly rising to a first maximum within $\simeq 10$ d from the SN explosion. At $\simeq +34$ d both the $g-$ and $r-$band light curves show a further rise to a second and broader peak (lasting $\simeq 25$ d), while the $i-$band light curve does not reveal the same 'double-peaked' shape due to lack of early observations in this band. After the second peak ($t \gtrsim 60$ d), the photometric evolution is slower in all bands, with decline rates of $\simeq 0.012$, 0.011 and 0.013 mag d^{-1} in $g-$, $r-$ and $i-$band, respectively. The rise times in g and r were computed fitting the early evolution in each band with a second-order polynomial in order to estimate the epoch of the maximum in each band. These were computed as $t_{max} - t_{expl}$, giving $t_{rise,g} = 7.9 \pm 1.5$ and $t_{rise,r} = 10.7 \pm 1.5$ d, where the errors are completely dominated by the uncertainty on the explosion epoch. These rise times are slightly faster than the average $r-$band rise time inferred by Taddia et al. (2015) and Taddia et al. (2019) for their samples of SNe Ic-BL ($\simeq 14.7$ and $\simeq 15$ d, respectively), although still comparable with the faster end of the SN Ic-BL iPTF rise-time distribution presented in Taddia et al. (2019, their fig. 17). We note, in addition, that the photometric evolution during the rise is well reproduced by power-laws of the form $L_g \propto t^{0.29}$ and $L_r \propto t^{0.41}$ erg s^{-1}, with fluxes in g and r computed using the zero-points for the ZTF filters reported by the Spanish Virtual Observatory (SVO[10]; Rodrigo et al. 2012).

The $g - r$ early (i.e., at $t \lesssim 10$ d) color evolution is relatively fast, with the color index increasing from $\simeq 0.15$ to $\simeq 0.60$ mag. At $t \gtrsim 10$ d, the $g - r$ index evolves toward bluer colors until $\simeq +80$ d, thereafter remaining roughly constant ($\simeq 0.1$ mag) throughout the rest of the photometric evolution of SN 2018ijp. At $t \gtrsim +60$ d, we note an almost linear decline in $r - i$, with the color index becoming progressively bluer with time, as reflected by the evolution of the pseudo-continuum observed in the spectra of SN 2018ijp (see Sect. 3.2).
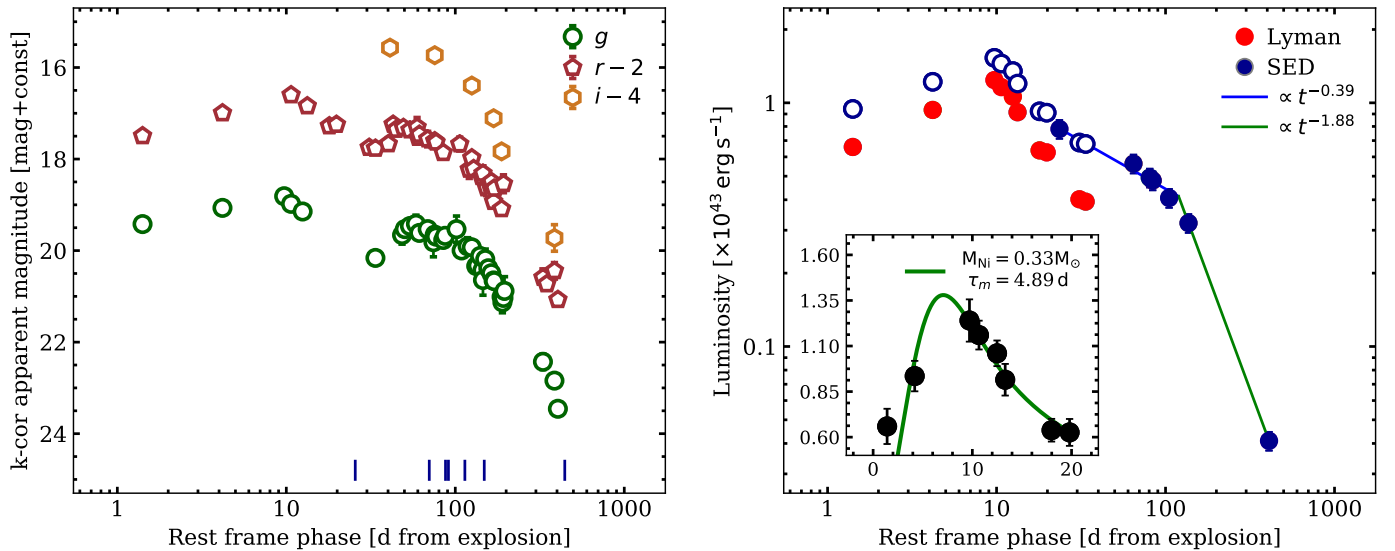
Absolute magnitudes were obtained, after correcting apparent values for the Galactic reddening and adopting a distance modulus $\mu = 37.85$ mag (see Sect. 1). The resulting $M_{r,peak}$ falls within the brighter end of the distribution of peak magnitudes presented in Taddia et al. (2019).

3.1.1. Evolution of the bolometric luminosity

The early ($t \lesssim +30$ d) bolometric light curve of SN 2018ijp was obtained following the prescriptions of Lyman et al. (2014, see their Eq. 6 for their sample of SE SNe), allowing an estimate of the $g-$band bolometric corrections from the evolution of the

---

[8] http://graspa.oapd.inaf.it/foscgui.html
[9] obtained under programme 0102.D-0221 (P.I. Sollerman).

[10] http://svo2.cab.inta-csic.es/svo/theory/fps3/

Fig. 2. Left: The *gri* light curves of SN 2018ijp, k-corrected apparent magnitudes versus rest frame days. Blue ticks at the bottom mark the epochs of spectroscopic observations. **Right:** Bolometric light curve of SN 2018ijp estimated following the prescriptions of Lyman et al. (2014) (red points) and by fitting the SEDs obtained from the spectra (solid blue points). An estimate of the early peak obtained matching the luminosities obtained at $\simeq +34$ d is also shown (open blue points). The inset shows the fit of the model of Arnett (1982) to the early luminosity evolution of SN 2018ijp, resulting in $M_{Ni} \simeq 0.3\,M_\odot$ and $\tau_m \simeq 4.9$ d, corresponding to $E_k \simeq 3.3 \times 10^{51}$ erg and $M_{ej} \simeq 0.7\,M_\odot$.

$g-r$ color. The resulting light curve peaks at $\simeq 1.24 \times 10^{43}$ erg s^{-1}, with the maximum occurring at $t_{peak}^{bol} \simeq +9.7$ d. The total radiated energy is $\simeq 2.1 \times 10^{49}$ erg within the first 34 d.

An alternative estimate of the luminosity can be obtained using the information on the spectral energy distribution (SED) available through the analysis of the spectra at $t \geq +24$ d. We computed *BVRI* and *gri* synthetic photometry using the CAL-CPHOT task available through the IRAF/STSDAS Synthetic Photometry (SYNPHOT) package and fitted black body (BB) functions to the resulting SEDs. Final luminosities were then obtained integrating the fluxes in each band excluding the spectral region at wavelengths shorter than 2000 Å, where the flux is expected to be suppressed by line blanketing (see, e.g., Nicholl et al. 2017). Assuming a power-law decline at $t \gtrsim 30$ d (see Fig. 2; right panel), and interpolating the bolometric light curves at the same phases, we estimated an offset of 2.85×10^{42} erg s^{-1} between the two methods, as computed at +34 d. Applying this offset to the early light curve would give a peak luminosity of $\simeq 1.5 \times 10^{43}$ erg s^{-1} with a total radiated energy of $\simeq 2.8 \times 10^{49}$ erg within the first 34 d and $\simeq 1.4 \times 10^{50}$ erg during the 410 d covered by our follow-up campaign.

A comparison of the +24 d spectrum with the SN templates included in the SuperNova IDentification (SNID[11]; Blondin & Tonry 2007) tool and the GEneric cLAssification TOol (GELATO[12]; Harutyunyan et al. 2008), gives a good match with SNe Ic/Ic-BL, with a particular good match with SNe 2004aw and 1998bw around peak (see Sect. 4). In the following, we will therefore compare the main observables of SN 2018ijp at $t \lesssim 20$ d with quantities inferred from samples of SNe Ic-BL, and conduct simple modeling of such an early light curve. Following Lyman et al. (2016, their Eq. 4), the average peak luminosity obtained with the methods described above already suggests a relatively high mass of ^{56}Ni expelled by the SN explosion (M_{Ni}

$\simeq 0.57\,M_\odot$), although comparable to the average value found by Drout et al. (2011) for their sample of SNe Ic-BL.

The total mass and the kinetic energy of the ejecta can be derived following the prescriptions of Arnett (1982) (see also the formulation of Wheeler et al. 2015 of the analytical model applied to a sample of SE SNe). The model assumes spherical symmetry, a constant optical opacity κ_{opt}, small initial radius ($R_0 \ll 10^{14}$ cm) and homologous expansion of the optically thick ejecta $R(t) = R_0 + v_{sc}t$, with v_{sc} being the scale expansion velocity (see Arnett 1982). Under these assumptions, the characteristic time scale $\tau_m = \sqrt{2\tau_0\tau_h}$ can be defined, with τ_0 and τ_h being the diffusion and hydrodynamical times, respectively (see Wheeler et al. 2015).

The evolution of the bolometric luminosity can be expressed as a function of the kinetic energy of the ejecta E_k, the ^{56}Ni mass $M_{^{56}Ni}$ and the total mass of the ejecta M_{ej} as follows (see Chatzopoulos et al. 2012):

$$L(t) = M_{^{56}Ni}\, e^{-x^2} \left[2\,(\epsilon_{^{56}Ni} - \epsilon_{^{56}Co}) \int_0^x \xi e^{-\xi\frac{\tau_m}{\tau_{Ni}+\xi^2}}\,d\xi + \right.$$
$$\left. \epsilon_{Co} \int_0^x \xi e^{-\xi\frac{\tau_m}{\tau_{Ni}}\left(1 - \frac{\tau_{Co}-\tau_{Ni}}{\tau_{Co}\tau_{Ni}}\right)+\xi^2}\,d\xi \right], \quad (1)$$

where $x \equiv t/\tau_m$, $\epsilon_{Co} = 6.78 \times 10^9$ erg s^{-1} g^{-1} and $\epsilon_{Ni} = 3.90 \times 10^{10}$ erg s^{-1} g^{-1} (see, e.g., Cappellaro et al. 1997) and τ_{Co}, τ_{Ni} are the radioactive decay times of ^{56}Co and ^{56}Ni (111.3 and 8.8 d, respectively; see, e.g., Nadyozhin 1994). Assuming a constant optical opacity $\kappa_{opt} = 0.07$ cm^2 g^{-1} (Chugai 2000) and fitting Eq. 1 to the bolometric light curve of SN 2018ijp gives $M_{^{56}Ni} = 0.33 \pm 0.05\,M_\odot$ and $\tau_m = 4.89 \pm 0.80$ d. Assuming a uniform density within the ejecta, τ_m can also be expressed as follows:

$$\tau_m = \left(\frac{2\kappa_{opt}}{\beta c}\right)^{1/2} \left(\frac{3\,M_{ej}^3}{10\,E_k}\right)^{1/4}, \quad (2)$$

where β is an integration constant ($\beta \simeq 13.8$, as in Wheeler et al. 2015). The degeneracy between the kinetic energy and the to-
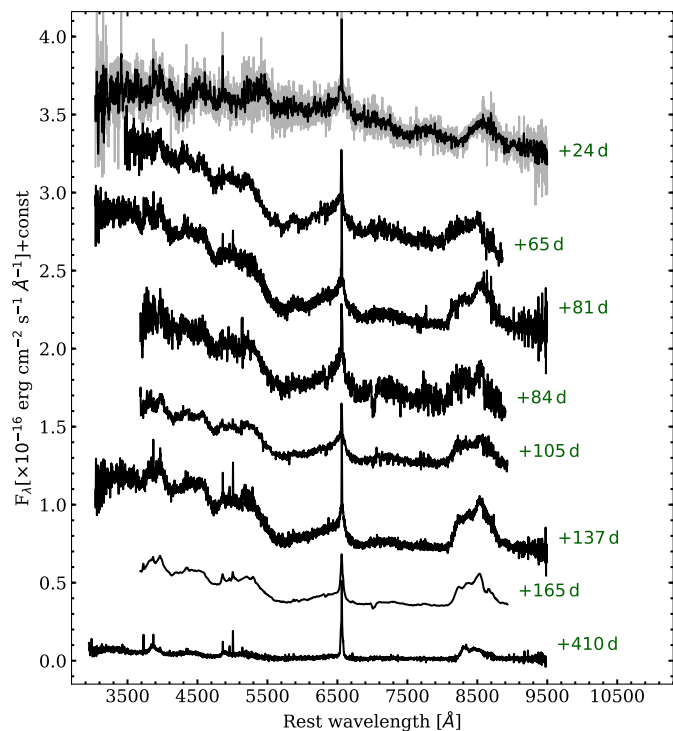
Fig. 3. Spectral sequence of SN 2018ijp. Rest frame phases refer to the estimated epoch of the explosion. The +165 d spectrum has been degraded to the resolution of the +105 d spectrum, to facilitate the comparison. The +24 d spectrum has been degraded to 1/3 of its resolution and plotted in black, while the original spectrum is reported in gray.

Fig. 4. Evolution of the Hα profile, along with a multi-component fit.

tal mass of the ejecta $E_k = 1/2 M_{ej} < v^2 >$, with $< v^2 >$ being the mean squared expansion velocity, can be broken assuming uniform density within the expanding ejecta and hence $< v^2 >= 3/5 v_{ph}^2$ (Arnett 1982), where v_{ph} is the photospheric velocity. An estimate of $< v >$ can be obtained measuring the minima of the P-Cygni absorption profiles of Fe II or O I lines around maximum light (see, e.g. Dessart et al. 2016), which, in the case of SN 2018ijp, corresponds to $v_{O I} \simeq 12400 \, \mathrm{km \, s^{-1}}$ at $\simeq +24 \, \mathrm{d}$ (see Sect. 3.2). Following Dessart et al. (2016), this corresponds to $< v > \simeq 21200 \, \mathrm{km \, s^{-1}}$. Taking this value for the mean expansion velocity, Eq. 2 gives $M_{ej} = 0.73 \pm 0.05 \, M_\odot$ and $E_k = (3.26 \pm 0.17) \times 10^{51}$ erg for the total mass and the kinetic energy of the ejecta.

The derived values are similar to those found by Taddia et al. (2019) for their sample of SNe Ic-BL, with an ejected mass comparable to that found for PTF11lbm using a similar approach. However, the ^{56}Ni mass is higher, corresponding to $\sim 45\%$ of M_{ej}. While these values do not make of SN 2018ijp the most extreme case (see, e.g., the values found for iPTF16asu), the relative amount of nickel is uncomfortably high and might suggest a non-negligible contribution of ejecta-CSM interaction to the total luminosity also around the first peak of SN 2018ijp.

The bolometric light curve, as constructed from the spectra, can be reproduced by a 'broken power-law' starting from +24 d (Fig. 2, right panel), with the break occurring at $\simeq +120 \, \mathrm{d}$. A similar behavior is observed in interacting transients, where the SN shock is expected to break through a dense and extended pre-existing CSM (see, e.g., Fransson et al. 2014; Ofek et al. 2014b; Tartaglia et al. 2020, and references therein). The total radiated energy up to +410 d, as well as the prominent narrow Hα line visible at all phases also support a CSM interaction interpretation
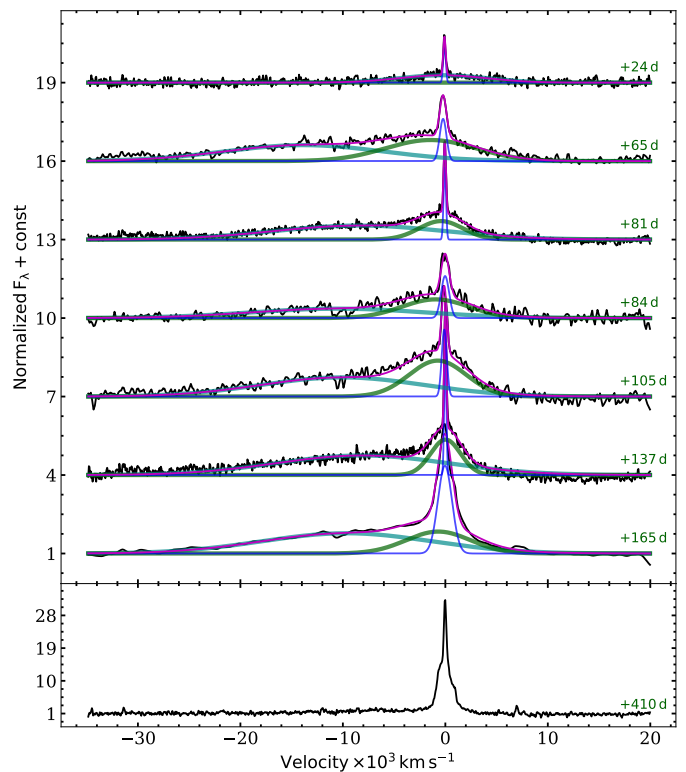
for the second peak of SN 2018ijp. In the case of SN 2018ijp, at least a fraction of the luminosity output during the first peak could also be powered by interaction of the SN ejecta. A more complex modeling, beyond the scope of this paper, is probably required to properly model the evolution of SN 2018ijp in order to estimate its explosion parameters.

3.2. Spectroscopy

3.2.1. Low resolution spectroscopy

Low- and medium-resolution optical spectra, calibrated against photometry obtained at the closest epochs, are shown in Fig. 3. At +24 d, the spectrum shows un-resolved Balmer lines in emission (Hα and Hβ) on top of shallower broader features. The lack of other narrow emission lines typically associated with H II regions (e.g., [O III], [O II] and [N II]) would suggest that these are recombination lines arising from an un-shocked CSM, although the signal–to–noise (S/N) ratio of the spectrum is not sufficient to rule out the presence of such lines (see Sect. 3.2.2). Blends of Fe II lines are likely responsible for the "bumps" observed between 4000 and 5000 Å (multiplets 26, 27, 28, 37 and 38) and at ~ 5300 Å (multiplets 42, 48 and 49), making a direct estimate of the ejecta photospheric velocity (through the Fe II λ5169 line; Dessart & Hillier 2005) difficult. On the other hand, at $\lambda \gtrsim 7000$ Å the spectrum shows broader features of O I $7772 - 7775$ Å. From the minimum of the O I P-Cygni absorption we inferred an expansion velocity of $\simeq 12400 \, \mathrm{km \, s^{-1}}$, with the blue wing extending to $\simeq 2 \times 10^4 \, \mathrm{km \, s^{-1}}$, which, following the discussion in Dessart et al. (2016), corresponds to a mean expansion velocity of $\simeq 21200 \, \mathrm{km \, s^{-1}}$. At the same epoch, and throughout the spectroscopic evolution of SN 2018ijp covered by our follow-up campaign, we also detect the near in-

frared (NIR) Ca II triplet (see Fig. 3). The +65 d spectrum reveals a significant evolution, with the continuum becoming apparently much bluer. The total luminosity of Hα (measured in the $6000 - 7000$ Å range) at +65 d ($\simeq 1.1 \times 10^{41}$ erg s^{-1}) also shows a drastic increase with respect to the previous epoch ($L_{H\alpha,+24\,d} \simeq 2.8 \times 10^{40}$ erg s^{-1}), subsequently remaining roughly constant up to +137 d. While blue excesses can be generally associated with the contribution of fluorescence from numerous blended Fe lines (see, e.g., Tartaglia et al. 2020, and references therein), an increase in the temperature of the pseudo-continuum can also be interpreted as a result of ongoing ejecta-CSM interaction. This interpretation would also be supported by the shape of the bolometric light curve (Fig. 2, right panel), showing a "broken power-law" shape typical of interacting SNe. A "delayed" interaction might be explained by the presence of a confined dense shell surrounding the progenitor star of SN 2018ijp. Based on the evolution of the bolometric luminosity and the results discussed in Sect. 3.1.1, as well as on the Hα evolution discussed below, we can assume that the onset of ejecta-CSM interaction is at $t \gtrsim +24\,d$. A constant expansion velocity of $v \simeq 21200$ km s^{-1} (see above) would place the shell at a distance of $\simeq 4.4 \times 10^{15}$ cm from the progenitor star of SN 2018ijp. This estimate is of the same order of magnitude as that inferred from the BB fit performed at +65 d ($\simeq 10^{15}$ cm). Assuming that the SN shock breaks through the confined shell roughly at $t \simeq 120$ d (i.e., when the break in the power-law describing the light curve occurs), this would imply an external radius of the shell of $\simeq 2.2 \times 10^{16}$ cm. Such a detached H-rich shell might be produced by a single massive progenitor and hence expelled $20 - 100$ yr before CC, assuming a $v_{wind} \simeq 70$ km s^{-1}, as estimated in Sect. 3.2.2 (see also Margutti et al. 2017, for a similar interpretation for SN 2014C), or the last eruptive episode of a Wolf-Rayet star in its transitional phase from the LBV phase (see, e.g., the case of the Type Ibn SN 2006jc; Pastorello et al. 2007), but could also originate from a H-rich companion through a stationary wind or an eruptive event (see Sect. 5).

In Fig. 4 we show the evolution of the spectral region around Hα, revealing a structured and asymmetric profile throughout the spectroscopic evolution of the transient. At +24 d, the overall profile is well reproduced by a broad, blue-shifted component with a FWHM $\simeq 10^4$ km s^{-1} and a narrow unresolved component (FWHM < 70 km s^{-1}) centered at Hα rest wavelength, although a comparison with early spectra of the Type Ic-BL SN 1998bw might suggest a different interpretation for this feature (see Sect. 4). A multi-gaussian fit between +65 and +165 d reveals two broad components: a blue-shifted component with a FWHM of $\simeq 2 \times 10^4$ km s^{-1} and a redder one with a FWHM slowly decreasing from $\simeq 10^4$ to $\simeq 3 \times 10^3$ km s^{-1}, with a third narrow and unresolved component. While the redder component is likely due to the wings of the typical electron scattering profile observed in high-resolution spectra of interacting transients (see, e.g., Huang & Chevalier 2018), the corresponding velocity width is also consistent with those observed in shocked regions of dense media typically surrounding the progenitors of SNe IIn. A clumpy (e.g., Chugai & Danziger 1994) or highly asymmetric (e.g., Smith et al. 2014) CSM, could explain the simultaneous presence of a broad component, which would then be produced by the outer ionized layers of the freely expanding SN ejecta and an intermediate component arising from the shocked CSM, with the narrow emission feature possibly produced in the ionized un-shocked CSM (see, e.g. Turatto et al. 1993, although see Sect. 3.2.2 for a possible different interpretation of the Hα profile observed at $t \gtrsim +65$ d). By +410 d, the shape of Hα has changed significantly, showing a narrow component on top of a

boxy, flat-topped line profile, reminiscent of the overall profile observed in H-rich interacting SNe IIn (see, e.g., Taddia et al. 2020, and the discussion in Sect. 5) and is not well reproduced by a combination of Gaussian profiles.

3.2.2. The X-shooter spectrum

Medium resolution spectra were obtained with X-shooter on 2019 May 4.06 UT (JD = 2458607.56, $t = +165$ d). The observations consist of 4 exposures per arm, median combined to produce a single spectrum covering the $350 - 2000$ nm wavelength range[13]. Each observation was obtained at airmass $\lesssim 1.5$, with an average seeing of 0.″7 and we therefore take the nominal values of resolution for each arm (R $\equiv \lambda/\Delta\lambda = 5400$, 8900 and 5600 in the UVB, VIS and NIR arm, respectively, for slit widths of 1.″0 in UVB and 0.″9 in VIS and NIR)[14]. These are consistent with the resolutions measured from the available sky lines. The resulting spectra are shown in Fig. 5.

The Hα region shows a structured profile with a narrow (FWHM $\simeq 70$ km s^{-1}) and an "intermediate" (FWHM $\simeq 7400$ km s^{-1}) component, both centered at Hα rest wavelength, on top of a broader (FWHM $\simeq 21500$ km s^{-1}) blue-shifted ($v_{shift} \simeq 10600$ km s^{-1}) component (see also Fig. 4). A much shallower broad component is observed in Hβ, with a FWHM of $\simeq 2130$ km s^{-1} and an unresolved narrow component (FWHM < 60 km s^{-1}.)

The measured Hδ/Hβ and Hγ/Hβ line ratios of the narrow components are $\simeq 0.2$ and 0.5, roughly corresponding to the predicted Balmer decrement in a Case B recombination scenario (assuming $T = 10^4$ K and $n_e = 10^2$ cm^{-3}; see Osterbrock & Ferland 2006), consistent with negligible contribution of the local environment to the total extinction in the direction of SN 2018ijp. The electron density was inferred from the [O II] line ratio ($j_{3729}/j_{3726} = 1.26$, corresponding to $n_e \simeq 10^2$ cm^{-3}, see Osterbrock & Ferland 2006), as well as from the [S II] j_{6716}/j_{6732} ratio, giving the same result. The narrow Hα/Hβ ratio of $\simeq 3.5$ is somewhat higher than that predicted in the case B scenario, which might suggests some contribution from the transient to Hα. A number of other narrow lines are also detected, including [O II] λλ3726, 3729, [O III] λλ4363, 4958 and 5007, [Ne III] λλ3868, 3967, [S II] λλ6716, 6732 and [N II] λλ6548, 6583, which, along with the narrow Balmer lines are all below the resolution limit, with the exception of Hα narrow component, showing a FWHM $\simeq 70$ km s^{-1}.
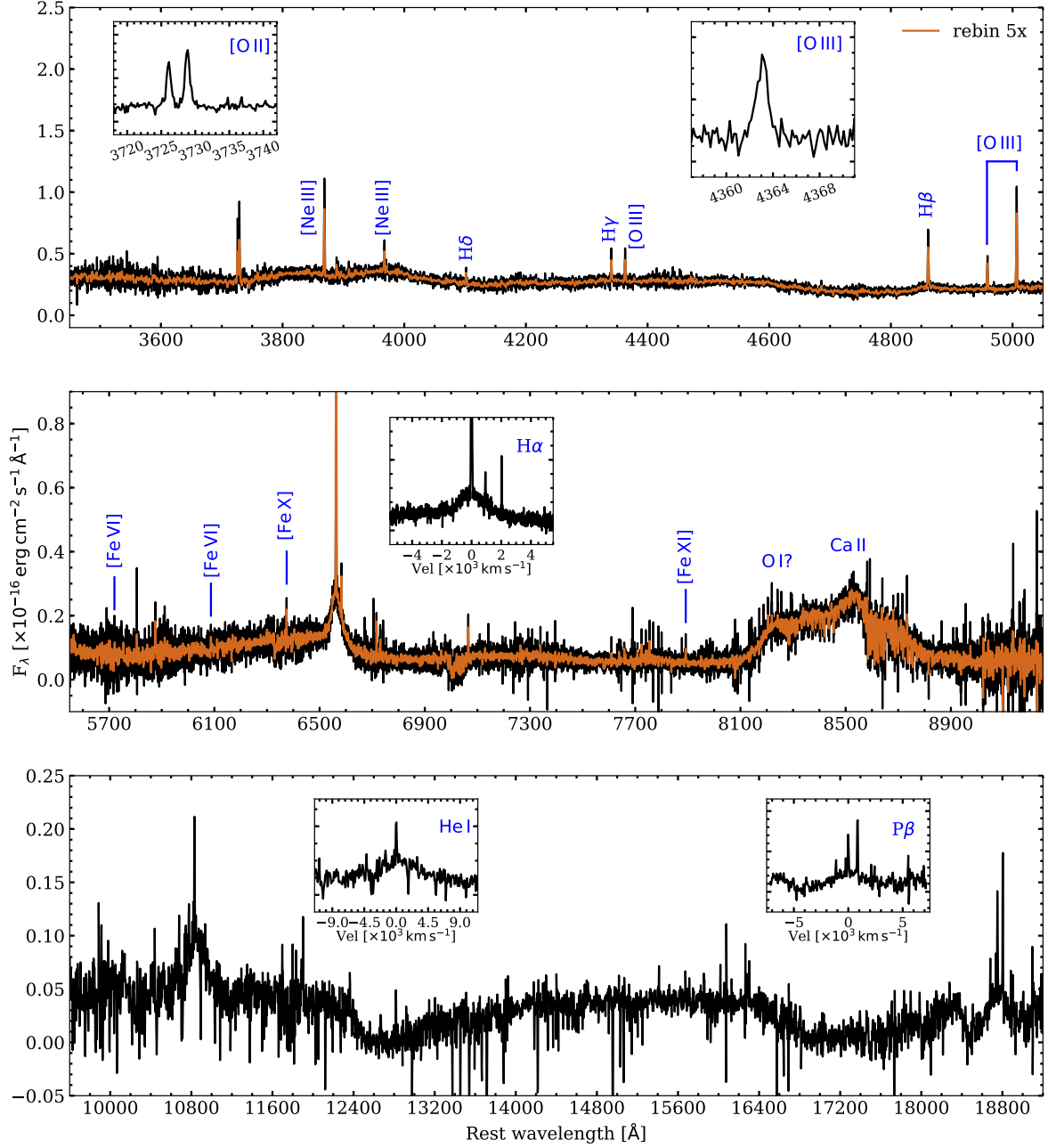
Following the line identification of Fransson et al. (2002), we also detect unresolved high ionization narrow lines, such as [Fe XI] λ7892, [Fe X] λ6375, [Fe VI] λ5720, 6087 and 5276 as well as narrow He I λ3889 and 7065.

As highlighted in Figs. 3 and 5, the non-detection of such features at earlier phases is most likely due to the lower S/N and resolution of the spectra. As in SN 1995N (see also Sollerman et al. 2020), these features can be interpreted as arising from the dense circumstellar gas. These lines are significantly fainter at +410 d where the S/N and resolution of the spectrum is still sufficient to detect such features.

The [O III] λ4363 is clearly detected in the X-shooter spectrum. This line is usually faint compared to [O III] λλ4959, 5007, with $(j_{5007} + j_{4959})/j_{4363} \gtrsim 50$ in typical H II regions. The inferred value $(j_{5007} + j_{4959})/j_{4363} = 7.2$ implies very high temperatures

---

[13] https://www.eso.org/sci/facilities/paranal/instruments/xshooter/overview.html
[14] https://www.eso.org/sci/facilities/paranal/instruments/xshooter/inst.html

Fig. 5. X-shooter spectra of SN 2018ijp obtained at +165 d. **Top** panel shows insets with zoom-ins of the [O ɪɪ] $\lambda\lambda 3726, 3729$ and [O ɪɪɪ] $\lambda 4363$ regions. **Middle** and **bottom** panels show insets of the Hα, He ɪ $\lambda 10830$ and Paα regions in velocity space. The NIR spectrum has been re-rebinned to a fifth of its resolution to facilitate the identification of the main emission features.

and densities for the emitting gas (e.g., $T_e \gtrsim 2.7 \times 10^4$ K for electron densities $n_e \gtrsim 10^6$ cm^{-3} in a 5-level atom approximation; see De Robertis et al. 1987; Shaw & Dufour 1995), suggesting a circumstellar origin for the [O ɪɪɪ] lines as well. This could imply a [O ɪɪɪ] flux arising from different regions (i.e., both from an underlying H ɪɪ region and the CSM). Alternatively, narrow features, such as [O ɪɪ], [O ɪɪɪ] and [S ɪɪ], might all have circumstellar origin, along with Fe high ionization features, with different lines mapping regions with different densities. A similar behavior is observed in H ɪɪ regions, where [O ɪɪ] lines are thought to arise from outer regions of the nebula, whereas [O ɪɪɪ] features are produced from more uniformly distributed gas (see, e.g., Nicholls et al. 2014, and references therein).

In order to further explore these different scenarios, we inspected the 2D X-shooter frames, which suggested a common origin for at least the [O ɪɪ] and the narrow Balmer lines, with spatially extended emission suggesting contamination from the environment of SN 2018ijp. The [O ɪɪɪ] and the high ionization Fe lines, on the other hand, do not show a similar spatially extended emission, favoring a circumstellar origin. The evolution of the narrow lines over the remaining ~ 300 d of our spectroscopic coverage also seems to support a circumstellar origin at least for the high ionization Fe lines, with have fluxes which decrease significantly from +165 to +410 d.
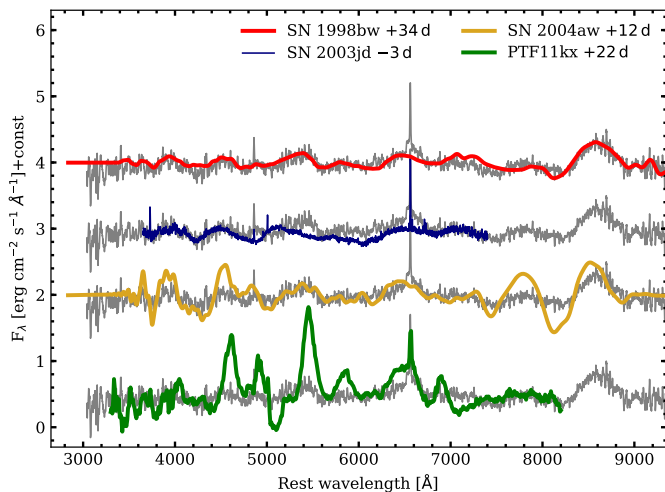
Fig. 6. The +24 d spectrum (16 d after $r-$band maximum, shown in grey) compared to "best-match" templates obtained with the SNID (Type Ic SN 2004aw and Ic-BL SN 1998bw) and GELATO (Ic SN 2003jd) classification tools. Spectra of SNe 2004aw and 1998bw are the "flattened" templates included in the SNID database. Phases relative to maximum light of each object are reported in the legend. The spectral continua of SNe 2018ijp and 2003jd (not included in the SNID template database) were estimated through *spline* functions and subtracted. The spectrum of SN 2018ijp has been smoothed in order to highlight its broad features.

4. On the nature of SN 2018ijp

Since spectra at $t \geq +65$ d are dominated by interaction, we use the one obtained at +24 d (i.e. 16 d after the first $r-$band peak) to investigate the nature of the explosion of SN 2018ijp. Our approach is based on automatic comparisons of the observed spectrum with the databases of SNID (based on the correlation techniques of Tonry & Davis 1979) and GELATO tools. SNID, in particular, is able to clip narrow emission lines at a specified redshift, in order to avoid spurious correlation peaks. Using this option in order to avoid contamination from the narrow Hα component, we get the best match with the Type Ic SN 2004aw (Taubenberger et al. 2006) 12 d after maximum, although the comparison also suggests many other Type Ic/Ic-BL SNe as good matches to the spectral features of SN 2018ijp, including the Type Ic-BL SN 1998bw (see Fig. 6, where we also include a comparison with the Type Ia-CSM PTF11kx around peak, disfavoring such a classification for SN 2018ijp). A similar result was obtained using GELATO, giving the best match with the Type Ic-BL SN 2003jd (Valenti et al. 2008) around maximum light. These comparisons thus suggest a SE SN classification for SN 2018ijp. In Fig. 7 (also including the peculiar Ic SNe 1997ef Iwamoto et al. 2000; Mazzali et al. 2000), on the other hand, we show that the first peak of SN 2018ijp resemble the photometric evolution of PTF11kx (see the inset), with similar absolute magnitudes and fast rise to maximum, although SN 1998bw also gives a good match at $t \gtrsim -10$ d (with respect to the $r-$band peak). Around the second peak, SN 2018ijp shows a different evolution with respect to all other comparison objects with the possible exception of PTF11kx, although its sampling is not as good as the one provided by our follow-up campaign between 20 d $\lesssim$ t $\lesssim$ 220 d. Based on this similarity, and since Ia-CSM SNe can also produce spectra similar to SN 2018ijp around the first peak, we further investigate the nature of SN 2018ijp by
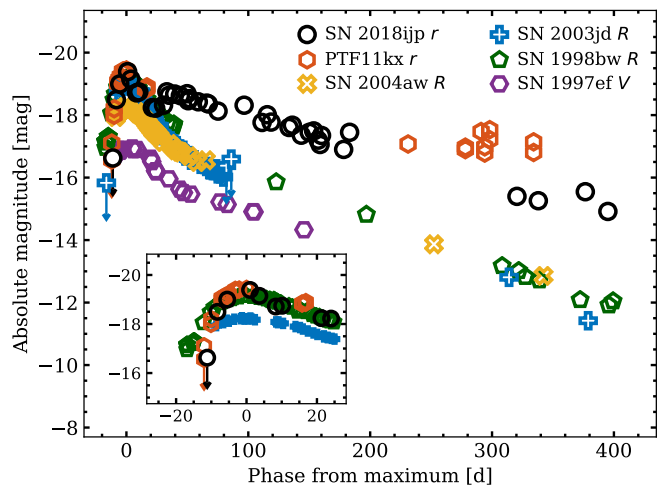
Fig. 7. Comparison of the absolute $r-$band light curve of SN 2018ijp with those of a number of other SNe. The sample was chosen based on comparison of the +24 d spectrum (see Fig. 6). The choice of the reported bands is given in the legend and was made based on the available photometric data for each object. In the inset, a comparison of the early $r-$band light curve of SN 2018ijp with those of SNe 2003jd, 2004aw, 1998bw and PTF11kx.

extending the comparison to transients of different nature, as described below.

Following Aldering et al. (2006), we compared the +24 d spectrum of SN 2018ijp (i.e., $\simeq$ 16 d after maximum) with "diluted" spectra of SN 1991T (Filippenko et al. 1992; Mazzali et al. 1995; Gómez & López 1998; Silverman et al. 2012) around peak. This choice is based on the claim that SNe Ia-CSM seem to show an association with 91T-like transients (see, e.g., Hamuy et al. 2003; Aldering et al. 2006; Prieto et al. 2007; Taddia et al. 2012). Spectra of SN 1991T around maximum were diluted using a black-body in order to simulate the effects of interaction – including a constant factor to account for the different distances and luminosities of the two objects – and the "best-fit model" was determined through a simple χ^2 minimization routine. A similar approach was adopted by Leloudas et al. (2015) to test how interaction would affect the appearance of SN spectra and their classification, although we did not include narrow Balmer lines (i.e., Hα) in our fit. In Fig. 8, we show the results of this fitting procedure, giving a good match with SNe 2004aw and 1998bw and thus confirming the results obtained with SNID, while the best-fit spectrum obtained with SN 1991T does not seem to reproduce well the broad features observed in SN 2018ijp. We note that a good match with SN 2004aw is obtained even without including a BB in the fitting procedure, suggesting that the interaction does not significantly shape the pseudo-continuum of SN 2018ijp around the first peak. This is also the rationale for our light curve analysis in Sect. 3.1.1.

At later phases (i.e. $t \geq +65$ d), we could not find a good match with any template spectrum either using SNID or GELATO, although, after clipping the narrow Hα component, GELATO suggests a marginal similarity with the Type Ib SN 2009er. The same result was obtained also diluting spectra of SNe 1991T, 1998bw and 2004aw, as detailed above. At the same time, we also note that the late spectral evolution of SN 2018ijp is different than that of the aforementioned transients (see Fig. 9), although, at +410 d, we note a remarkable similar-
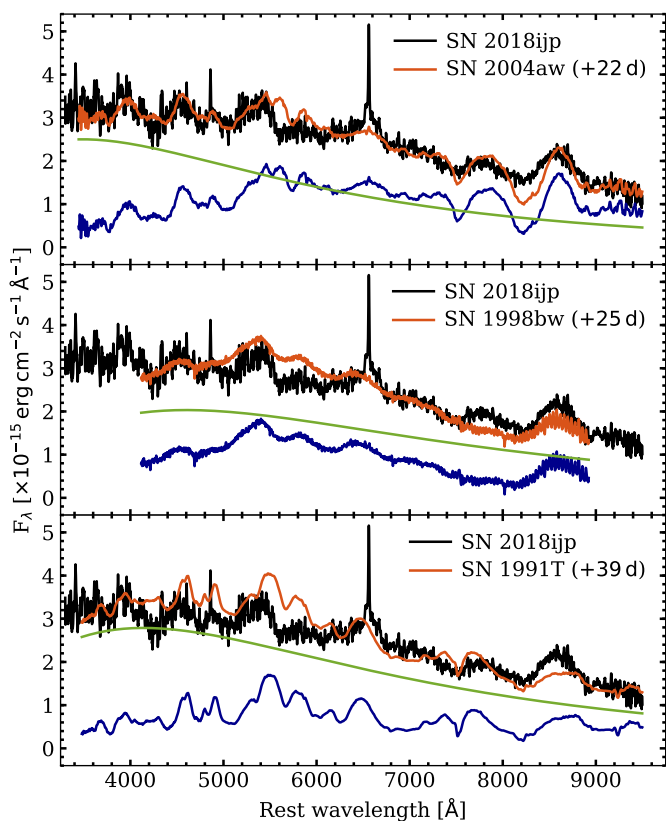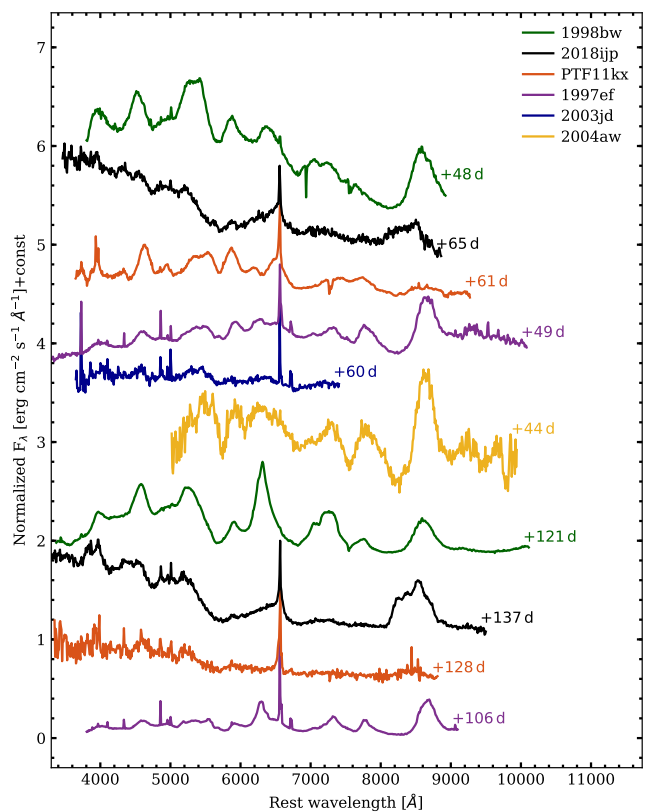
Fig. 8. Best fit models obtained using spectra of the Type Ic SNe 2004aw, Ic-BL 1998bw and Ia 1991T, adding a BB to the comparison objects. Blue scaled spectra are those of the comparison objects, while green lines are the BBs required to get the "best-fit" diluted spectra (see the main text for details). The spectrum of SN 2018ijp is obtained at +24 d ($\simeq$ 16 d after maximum, in the rest frame). Phases refer to maximum light.

Fig. 9. Comparison of spectra of SN 2018ijp at selected epochs and spectra of the SNe discussed in the main text at similar phases. Phases refer to the epoch of maximum light.

ity with a late spectrum of PTF11k obtained at a similar phase (see Fig. 10). These evidences support our claim that later spectra are dominated by strong signatures of interaction (namely a very blue continuum, and the presence of several Fe II multiplets, with a prominent and structured Hα line in emission; see Fig. 4).

5. Summary and conclusions

We presented the peculiar photometric and spectroscopic evolution of SN 2018ijp and discussed its observables. The transient shows double-peaked $g-$ and $r-$band light curves with a fast-evolving first peak showing an evolution similar to those observed in the Type Ic-BL SN 1998bw and the Ia-CSM PTF11kx.

A comparison of the first spectrum, obtained at +24 d (around the first peak), with spectral templates included in commonly used classification tools (such as SNID and GELATO) favor a SE SN, providing good matches with the peculiar Type Ic SN 2004aw and the Ic-BL SN 1998bw (see Fig. 3). We could not find a good match with any SN Ia either with SNID or GELATO, or modeling the effects of ongoing ejecta-CSM interaction with a BB (see Sect. 4 and Fig. 8), which did not give a good match with a 91T-like SN, generally associated to SNe Ia-CSM (e.g., Leloudas et al. 2015). We note that the "template" spectrum of SN 2004aw $\simeq$ 22 d after maximum resemble that of SN 2018ijp even without introducing an extra component. Based

on this early spectral similarity, we model the early evolution of the bolometric luminosity of SN 2018ijp using the simple analytical model of Arnett (1982), suggesting a mass of expelled radioactive ^{56}Ni of $\simeq 0.3\,M_\odot$ with respect to a total ejected mass of $0.7\,M_\odot$ and kinetic energy of 3.3×10^{51} erg. This makes a reasonable match to SE SNe, with inferred values overall consistent with those found by Taddia et al. (2019) for their sample of SNe Ic-BL, and the mean nickel mass of the iPTF Ic SN sample ($0.2\,M_\odot$; Barbarino et al. 2020). We remark that this analysis is only meant to infer rough estimates and the resulting values have to be considered approximations of the real quantities. In addition, the very high fraction of radioactive ^{56}Ni to total ejected mass inferred for SN 2018ijp might suggest that interaction also plays a role in its early evolution, as possibly indicated by the presence of narrow emission lines superimposed on Ic-BL spectral features. In order to explain simultaneous signatures of interaction and SN features observed in the +24 d spectrum, we need to invoke a peculiar geometrical configuration for the CSM (e.g., a highly asymmetric explosion), a "clumpy" CSM (see, e.g., Chugai & Danziger 1994), a moderate amount of CSM (with respect to those expected in SNe IIn and Ibn) or a combination of the three. This would, however, affect the results of our modeling of the first peak of SN 2018ijp, although it still gives reasonable results compared to those obtained by Taddia et al. (2019) for their sample of SNe Ic-BL.

Inspection of the spectral region around the Hα line (Fig. 4), suggests the presence of a very broad, blue-shifted component, marginally visible since +24 d (see Fig. 3). Identifying this broad feature as H would be at odds with a SE SN origin, although the comparisons with SNe Ic-BL discussed in Sect. 4 (see, e.g.,
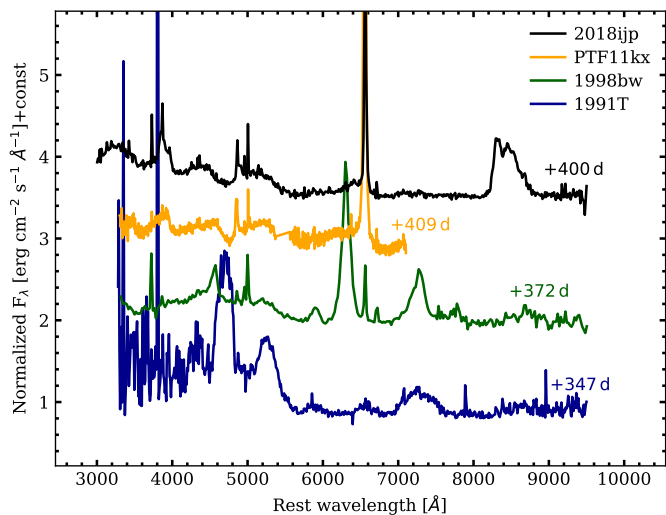
Fig. 10. Comparison of the late spectrum of SN 2018ijp obtained at +410 d ($\simeq$ 400 d after $r-$band maximum) with spectra of the SNe discussed in the main text. Phases refer to the epochs of maximum light.

Fig. 6) reveal that broad features at these wavelengths are also observed in SE SNe. At $t > +24$ d, the spectral evolution of SN 2018ijp is clearly dominated by signatures of interaction, as also highlighted by its late photometric evolution. In this context, the very high velocities inferred for the broad Hα component (see Fig. 4) at these phases could be explained with a high optical depth by incoherent electron scattering in the post-shock region. A combined effect of a high optical depth and shock velocity was discussed by Taddia et al. (2020, see their fig. 22) in order to explain the similarly structured Hα profile of SN 2013L. In this scenario, while the slope of the blue wing of Hα is strongly affected by the optical depth of the CSM, the suppression of the flux at redder wavelengths is caused by the efficient thermalization (obscuration) of the Hα photons in the SN ejecta. This scenario is also supported by the shape of Hα at +410 d, showing a boxy, flat-topped profile similar to that of SN 2013L, although with lower velocities, suggesting a lower expansion velocity of the shocked material. The match with the absolute light curve of PTF11kx at later phases, the dramatic evolution in the observed spectral continuum from +24 and +65 d (see Sect. 3.2 and Fig. 3) and the shape of the bolometric light curve at $t \gtrsim 25$ d (see Fig. 2, right panel) seem all to support a scenario where the late-time evolution of SN 2018ijp is dominated by ejecta-CSM interaction.

We therefore interpret the overall evolution of SN 2018ijp invoking two main phases, a first one dominated by radioactive decays, and an interaction-dominated phase where the SN ejecta collide with a H-rich pre-existing CSM (see Sect. 3.1.1), although we cannot exclude a contribution of CSM interaction also during the first phase. In this scenario, the early spectral features observed in SN 2018ijp, with high expansion velocities measured in the +24 d spectrum, as well as the relatively high mass of radioactive ^{56}Ni seem to suggest a stripped massive star, with the CSM either produced during a previous evolutionary stage or by a H-rich companion.

The location of the H-rich shell with respect to the center of the explosion and its estimated expansion velocity, on the other hand, is difficult reconcile with an outburst of a massive H-rich star subsequently exploding as a SE SN. A constant expansion velocity of 21200 km s^{-1} for the SN ejecta would give an inner radius of $\simeq 4 \times 10^{15}$ cm, with an outer layer extending up to $\simeq 2 \times 10^{16}$ (assuming $v_{wind} \simeq 70$ km s^{-1}, as inferred in Sect. 3.2.2). This would suggest that the mass-loss episode started ~ 100 Yr and lasted up to ~ 20 Yr before the explosion of the progenitor star. While a more accurate modeling of the observables is needed, a simple scenario might involve the presence of a H-rich companion as a possible source of the dense CSM needed to produce the observables of SN 2018ijp.

FOSCGUI is a graphic user interface aimed at extracting SN spectroscopy and photometry obtained with FOSC-like instruments. It was developed by E. Cappellaro. A package description can be found at http://sngroup.oapd.inaf.it/foscgui.html.

References

Abolfathi, B., Aguado, D. S., Aguilar, G., et al. 2018, ApJS, 235, 42
Aldering, G., Antilogus, P., Bailey, S., et al. 2006, ApJ, 650, 510. doi:10.1086/507020
Arnett, W. D. 1982, ApJ, 253, 785
Barbarino, C., Sollerman, J., Taddia, F., et al. 2020, arXiv:2010.08392
Bellm, E. C., Kulkarni, S. R., Graham, M. J., et al. 2019, PASP, 131, 018002
Ben-Ami, S., Konidaris, N., Quimby, R., et al. 2012, in Society of Photo-Optical Instrumentation Engineers (SPIE) Conference Series, Vol. 8446, Proc. SPIE, 844686
Blagorodnova, N., Neill, J. D., Walters, R., et al. 2018, PASP, 130, 035003
Blondin, S. & Tonry, J. L. 2007, ApJ, 666, 1024
Cappellaro, E., Mazzali, P. A., Benetti, S., et al. 1997, A&A, 328, 203
Cardelli, J. A., Clayton, G. C., & Mathis, J. S. 1989, ApJ, 345, 245
Chatzopoulos, E., Wheeler, J. C., & Vinko, J. 2012, ApJ, 746, 121
Chen, T. W., Inserra, C., Fraser, M., et al. 2018, ApJ, 867, L31
Chevalier, R. A. 1982, ApJ, 258, 790
Chevalier, R. A. & Fransson, C. 1994, ApJ, 420, 268. doi:10.1086/173557
Chugai, N. N. 2000, Astronomy Letters, 26, 797
Chugai, N. N. & Danziger, I. J. 1994, MNRAS, 268, 173
Crowther, P. A. 2007, ARA&A, 45, 177. doi:10.1146/annurev.astro.45.051806.110615
De Robertis, M. M., Dufour, R. J., & Hunt, R. W. 1987, JRASC, 81, 195
Dekany, R., Smith, R. M., Riddle, R., et al. 2020, PASP, 132, 038001
Dessart, L. & Hillier, D. J. 2005, A&A, 439, 671
Dessart, L., Hillier, D. J., Woosley, S., et al. 2016, MNRAS, 458, 1618
Drout, M. R., Soderberg, A. M., Gal-Yam, A., et al. 2011, ApJ, 741, 97
ESO CPL Development Team 2015, Astrophysics Source Code Library. ascl:1504.003
Filippenko, A. V., Richmond, M. W., Matheson, T., et al. 1992, ApJ, 384, L15. doi:10.1086/186252
Foley, R. J., Smith, N., Ganeshalingam, M., et al. 2007, ApJ, 657, L105
Fransson, C., Chevalier, R. A., Filippenko, A. V., et al. 2002, ApJ, 572, 350
Fransson, C., Ergon, M., Challis, P. J., et al. 2014, ApJ, 797, 118
Fremling, C., Sollerman, J., Taddia, F., et al. 2016, A&A, 593, A68
Gal-Yam, A. & Leonard, D. C. 2009, Nature, 458, 865. doi:10.1038/nature07934
Gómez, G. & López, R. 1998, AJ, 115, 1096. doi:10.1086/300248
Graham, M. J., Kulkarni, S. R., Bellm, E. C., et al. 2019, PASP, 131, 078001
Hamuy, M., Phillips, M. M., Suntzeff, N. B., et al. 2003, Nature, 424, 651
Harutyunyan, A. H., Pfahler, P., Pastorello, A., et al. 2008, A&A, 488, 383. doi:10.1051/0004-6361:20078859
Heger, A., Fryer, C. L., Woosley, S. E., Langer, N., & Hartmann, D. H. 2003, ApJ, 591, 288
Hogg, D. W., Baldry, I. K., Blanton, M. R., & Eisenstein, D. J. 2002, arXiv e-prints, astro
Hosseinzadeh, G., McCully, C., Zabludoff, A. I., et al. 2019, ApJ, 871, L9
Huang, C. & Chevalier, R. A. 2018, MNRAS, 475, 1261
Humphreys, R. M. & Davidson, K. 1994, PASP, 106, 1025. doi:10.1086/133478
Iwamoto, K., Nakamura, T., Nomoto, K., et al. 2000, ApJ, 534, 660
Kasliwal, M. M., Cannella, C., Bagdasaryan, A., et al. 2019, PASP, 131, 038003
Kuncarayakti, H., Maeda, K., Ashall, C. J., et al. 2018, ApJ, 854, L14
Leloudas, G., Hsiao, E. Y., Johansson, J., et al. 2015, A&A, 574, A61. doi:10.1051/0004-6361/201322035
Lyman, J. D., Bersier, D., & James, P. A. 2014, MNRAS, 437, 3848
Lyman, J. D., Bersier, D., James, P. A., et al. 2016, MNRAS, 457, 328
Margutti, R., Kamble, A., Milisavljevic, D., et al. 2017, ApJ, 835, 140
Masci, F. J., Laher, R. R., Rusholme, B., et al. 2019, PASP, 131, 018003
Maund, J. R., Pastorello, A., Mattila, S., et al. 2016, ApJ, 833, 128. doi:10.3847/1538-4357/833/2/128
Mazzali, P. A., Danziger, I. J., & Turatto, M. 1995, A&A, 297, 509
Mazzali, P. A., Iwamoto, K., & Nomoto, K. 2000, ApJ, 545, 407
Milisavljevic, D., Margutti, R., Kamble, A., et al. 2015, ApJ, 815, 120
Nadyozhin, D. K. 1994, ApJS, 92, 527
Nicholl, M., Guillochon, J., & Berger, E. 2017, ApJ, 850, 55
Nicholls, D. C., Dopita, M. A., Sutherland, R. S., Jerjen, H., & Kewley, L. J. 2014, ApJ, 790, 75
Ofek, E. O., Sullivan, M., Shaviv, N. J., et al. 2014a, ApJ, 789, 104
Ofek, E. O., Zoglauer, A., Boggs, S. E., et al. 2014b, ApJ, 781, 42
Oke, J. B., Cohen, J. G., Carr, M., et al. 1994, Low-Resolution Imaging Spectrometer for the Keck Telescope, Vol. 2198 (Society of Photo-Optical Instrumentation Engineers (SPIE) Conference Series), 178–184
Osterbrock, D. E. & Ferland, G. J. 2006, Astrophysics of gaseous nebulae and active galactic nuclei (University Science Books, 2006)
Pastorello, A., Cappellaro, E., Inserra, C., et al. 2013, ApJ, 767, 1
Pastorello, A., Smartt, S. J., Mattila, S., et al. 2007, Nature, 447, 829
Pastorello, A., Wang, X. F., Ciabattari, F., et al. 2016, MNRAS, 456, 853
Perley, D. A. 2019, PASP, 131, 084503
Prieto, J. L., Garnavich, P. M., Phillips, M. M., et al. 2007, arXiv:0706.4088
Rodrigo, C., Solano, E., & Bayo, A. 2012, SVO Filter Profile Service Version 1.0, IVOA Working Draft 15 October 2012
Schlafly, E. F. & Finkbeiner, D. P. 2011, ApJ, 737, 103
Schlegel, E. M. 1990, MNRAS, 244, 269
Shaw, R. A. & Dufour, R. J. 1995, PASP, 107, 896
Silverman, J. M., Foley, R. J., Filippenko, A. V., et al. 2012, MNRAS, 425, 1789. doi:10.1111/j.1365-2966.2012.21270.x
Silverman, J. M., Nugent, P. E., Gal-Yam, A., et al. 2013, ApJS, 207, 3
Smartt, S. J. 2009, ARA&A, 47, 63
Smith, N., Hinkle, K. H., & Ryde, N. 2009, AJ, 137, 3558
Smith, N., Mauerhan, J. C., & Prieto, J. L. 2014, MNRAS, 438, 1191
Sollerman, J., Fransson, C., Barbarino, C., et al. 2020, A&A, 643, A79. doi:10.1051/0004-6361/202038960
Steele, I. A., Smith, R. J., Rees, P. C., et al. 2004, in Proc. SPIE, Vol. 5489, Ground-based Telescopes, ed. J. M. Oschmann, Jr., 679–692
Taddia, F., Stritzinger, M. D., Phillips, M. M., et al. 2012, A&A, 545, L7. doi:10.1051/0004-6361/201220105
Taddia, F., Sollerman, J., Leloudas, G., et al. 2015, A&A, 574, A60
Taddia, F., Sollerman, J., Fremling, C., et al. 2019, A&A, 621, A71
Taddia, F., Stritzinger, M. D., Fransson, C., et al. 2020, A&A, 638, A92. doi:10.1051/0004-6361/201936654
Tartaglia, L., Pastorello, A., Sollerman, J., et al. 2020, A&A, 635, A39
Tartaglia, L., Pastorello, A., Sullivan, M., et al. 2016, MNRAS, 459, 1039
Taubenberger, S., Pastorello, A., Mazzali, P. A., et al. 2006, MNRAS, 371, 1459. doi:10.1111/j.1365-2966.2006.10776.x
Tonry, J. & Davis, M. 1979, AJ, 84, 1511. doi:10.1086/112569
Tonry, J. L., Stubbs, C. W., Lykke, K. R., et al. 2012, ApJ, 750, 99
Turatto, M., Cappellaro, E., Danziger, I. J., et al. 1993, MNRAS, 262, 128
Trundle, C., Kotak, R., Vink, J. S., et al. 2008, A&A, 483, L47. doi:10.1051/0004-6361:200809755
Valenti, S., Benetti, S., Cappellaro, E., et al. 2008, MNRAS, 383, 1485. doi:10.1111/j.1365-2966.2007.12647.x
Vernet, J., Dekker, H., D'Odorico, S., et al. 2011, A&A, 536, A105
Wheeler, J. C., Johnson, V., & Clocchiatti, A. 2015, MNRAS, 450, 1295
Wright, E. L. 2006, PASP, 118, 1711
Yoon, S.-C. & Cantiello, M. 2010, ApJ, 717, L62